Gate-controlled terahertz single electron photovoltaic effect in self-assembled InAs quantum dots

Y. Zhang[1,a)], K. Shibata[1,2,b)], N. Nagai[1], C. Ndebeka-Bandou[1,3], G. Bastard[1,3], and K. Hirakawa[1,2,c)]

[1] *Center for Photonics Electronics Convergence, Institute of Industrial Science, University of Tokyo, 4-6-1 Komaba, Meguro-ku, Tokyo 153-8505, Japan*

[2]*Institute for Nano Quantum Information Electronics, University of Tokyo, 4-6-1 Komaba, Meguro-ku, Tokyo 153-8505, Japan*

[3]*Laboratoire Pierre Aigrain, Ecole Normale Superieure, 24 rue Lhomond F75005, Paris, France*

(received:)

We have observed a terahertz (THz) induced single electron photovoltaic effect in self-assembled InAs quantum dots (QDs). We used a single electron transistor (SET) geometry that consists of a single InAs QD and nanogap electrodes coupled with a bowtie antenna. Under a weak, broadband THz radiation, a photocurrent induced by THz intersublevel transitions in the QD is generated even when no bias voltage is applied to the SET. The observed single electron photovoltaic effect is due to an energy-dependent tunneling asymmetry in the QD-SET. Moreover, the tunneling asymmetry changes not only with the shell, but also with the electron number in the QD, suggesting the manybody nature of the electron wavefunctions. The THz photovoltaic effect observed in the present QD-SET system may have potential applications to nanoscale energy harvesting.

---

a) Electronic mail: zhangya@iis.u-tokyo.ac.jp

b) Permanent address: Department of Electronics and Intelligent Systems, Tohoku Institute of Technology, Sendai 982-8577, Japan.

c) Electronic mail: hirakawa@iis.u-tokyo.ac.jp

Zero-dimensional nanostructures, such as self-assembled InAs quantum dots (QDs), are often called "artificial atoms" [1-3], because in such structures the electronic states are quantized into atom-like discrete energy levels. The single electron transistor (SET) structure [4], in which the source, drain, and gate electrodes are attached to a single zero-dimensional nanostructure, is an ideal platform to manipulate electronic structures and control transport properties even at a single electron level [5-10]. Since the typical orbital and charging energies in InAs QDs are about 10-40 meV[11] and lie in the terahertz (THz) range, the SETs that utilize an InAs QD as a Coulomb island are very attractive for exploring THz functions and devices.

Recently, we reported on THz intersublevel transitions in single InAs QDs. [12,13] By using a single electron transistor (SET) geometry that consisted of an InAs QD and nanogap metal electrodes coupled to a bowtie antenna, we could perform the intersublevel transition spectroscopy on a single InAs QD by measuring a photocurrent induced by the intersublevel transition and subsequent tunneling of photoexcited electrons in the QD. Sharp photocurrent peaks that originate from the intersublevel transitions in the QDs were observed in the Coulomb blockaded regions. Furthermore, as we will discuss later, we have found that there exist two mechanisms for the photocurrent generation, depending on the sequence of the escape of a photoexcited electron and the filling of an empty lower energy state.

Here, we report on the observation of a THz induced single electron photovoltaic effect in self-assembled InAs QDs. Under a weak, broadband THz radiation, a photocurrent induced by THz intersublevel transitions in the QD is generated even when no source-drain voltage, V_{DS}, is applied to the SET. We will discuss the observed photovoltaic effect in terms of an energy-dependent tunneling asymmetry intrinsic to the QD-SETs. Moreover, we will show that the tunneling asymmetry changes not only with the shell, but also with the electron number in the QD, suggesting the manybody nature of the electron wavefunctions. When a finite source-drain voltage is applied to the SET, the photocurrent is found to increase stepwise, which we attribute to

the blocking of electron tunneling by the electrodes. Implications of the single electron photovoltaic effect will be discussed in terms of nanoscale energy harvesting.

The self-assembled InAs QDs used in the present study were grown by molecular beam epitaxy on semi-insulating (100) and (211)B GaAs substrates. After successively growing a 300-nm-thick Si-doped GaAs layer, a 100-nm-thick undoped $Al_{0.3}Ga_{0.7}As$ barrier layer, and a 200-nm-thick undoped GaAs buffer layer, self-assembled InAs QDs were grown by depositing 4 monolayers of InAs at 480 °C. The QDs grown on the (100) surfaces had quasi-circular shapes with a diameter of about 90-100 nm and were slightly elongated in the [0-11] direction[14] (samples A and B), whereas the size of the QDs grown on the (211)B surfaces was typically (100-150)×(50-60) nm^2 (sample C).[15,16] Two Ti(5 nm)/Au(15 nm) electrodes separated by a 20-nm-gap were directly placed on an InAs QD and were used as the source and drain electrodes. A backgate voltage, V_G, was applied to the Si-doped GaAs buffer layer to change the electrostatic potential in the QD. The THz light source was a globar placed in a Fourier transform spectrometer. To tightly focus the THz radiation onto the samples, a hyper-hemispherical Si lens was placed on the back surface of the samples, as shown in Figure 1(a). A bow-tie antenna structure was also integrated with the nanogap electrodes to concentrate the THz field in the nanogap region[17]. All the measurements were performed at 4.6 K.

Figure 1(b) shows the Coulomb stability diagram of sample A. The white solid lines are eyeguides for the Coulomb diamonds. The numbers shown in the diamonds denote the number of electrons, N, in the QD. As seen in the figure, the Coulomb diamonds for the p- and d-shells are observed. Figure 1(c) shows the photocurrent induced by the broadband THz radiation measured as a function of V_G by applying a very small source-drain voltage (V_{DS} = 0.25 mV). This photocurrent is induced by the intersublevel transition in the QD[12]. The THz photocurrent measured on two other samples (samples B and C) are presented in Figures 1(e) and 1(g), respectively. Figure 1(h) shows the photocurrent measured as a function of V_{DS} on sample B at V_G = 1450 mV and 1550 mV. As seen in the figure, even when V_{DS} = 0, there is a finite photocurrent

through the QD. A similar behavior is observed for sample C measured at V_G = 510 mV, as shown in Figure 1(i). The non-zero THz-induced photocurrent at V_{DS} = 0 indicates that this photocurrent is induced by a photovoltaic effect. Then, the question is what is the origin of the asymmetry in the electron transport.

Figure 2(a) shows an energy band diagram of the QD-SET that schematically illustrates the mechanism for the photoexcitation. When the QD is illuminated with a broadband THz radiation, an electron in the lower energy state absorbs a photon and makes a transition to an upper energy state, leaving an empty state in the lower energy level. Then, the photoexcited electron tunnels to one of the electrodes, and the empty state is filled from the electrodes. The tunneling rate is required to be much higher than the relaxation rate to produce a photocurrent efficiently. Since the sublevel energy separation is typically 10-20 meV in our QD-SETs, the relaxation time is in the order of 100 ps-1 ns[18] and is much longer than the tunneling time (~10 ps) estimated from the transport measurements. Therefore, the effect of electron relaxation in the photocurrent generation is rather minor.

The tunnel coupling is determined by the effective distance between the electrode and the electron wavefunction in the QD[11]. Since the location of the QD in our samples is not well controlled with respect to the electrodes, we always have an asymmetry in the tunnel barriers between the QD and the source/drain electrodes. Now, let us consider a QD whose overlap with the source electrode is larger than that with the drain electrode. The effective tunneling barrier between the QD and the source electrode is thinner than that with drain electrode, as schematically shown in Figure 2(a). However, the tunnel asymmetry to the source and drain alone is not sufficient to induce a photovoltaic effect because the tunnel escape and filling from the same electrode cancel the net electron flow.

To explain the asymmetry, let us look into the electron wavefunctions in the QD. Let us assume a situation where the QD has a larger overlap with the source electrode. Because the size

of the electron wavefunction in the QD strongly depends on the shell, the tunnel coupling is also shell-dependent. Figures 2(b) and 2(c) respectively illustrate the numerical wavefunction patterns for the p- and d-states in the QD calculated by using *NEXTNANO*.[19] $\Gamma_{S(p)}$ and $\Gamma_{D(p)}$express the tunneling rate of the p-states to the source and drain electrodes, respectively. Similarly, $\Gamma_{S(d)}$and $\Gamma_{D(d)}$have the same meanings for the d-states. The wavefunction of the p-state is confined in the QD and its effective distance to the source electrode is smaller than that to the drain electrode, giving rise to a large tunneling asymmetry ($\Gamma_{S(p)} \gg \Gamma_{D(p)}$). Note that the tunnel coupling depends on the effective distance exponentially. On the other hand, because the d-states are more extended in the dot, the effective distances to the source and drain electrodes are not very different, which results in a smaller tunneling asymmetry ($\Gamma_{S(d)} > \Gamma_{D(d)}$). With increasing electron numbers, the electron wavefunctions become more complex. However, this increased complexity does not alter the fact that we always have a shell-dependent tunneling asymmetry in the QD-SET. Therefore, after photoexcitation, there is a non-zero probability that the photoexcited electron tunnels to one of the electrodes, but the empty state is filled from the other electrode, producing a net photocurrent through the QD-SET.

Now we wish to show that the tunneling asymmetry changes not only with the shell, but also with the electron number, N, in the QD. If we neglect higher-order tunneling processes, the electron number can change only by ±1 at one time in the single electron tunneling process due to Coulomb interactions in the QD. As previously reported, we showed that there exist two mechanisms for the photocurrent generation, *i.e.*, the $N \leftrightarrow N$-1 excitation and the $N \leftrightarrow N$+1 excitation processes[12]. For the $N \leftrightarrow N$-1 excitation, the photoexcited electron tunnels out first and the electron number is reduced to N-1 in the intermediate state. Then, an electron in the electrodes tunnels into the empty state and the SET returns to the initial state with N electrons, as shown in Figure 3(a). On the other hand, in the $N \leftrightarrow N$+1 excitation, an electron in the electrodes first tunnels into the QD to fill the lower empty state created by the photoexcitation and the electron number increases to N+1 in the intermediate state. Then, the SET goes back to the initial state by emitting the photoexcited electron to the electrodes, as shown in Figure 3(b). Since the $N \leftrightarrow N$-1 excitation

requires the upper energy state to lie above the Fermi levels of the source/drain electrodes, it generates a photocurrent in the pink colored regions of the Coulomb diamond shown in Figure 3(c). Similarly, since the N↔N+1 excitation needs to overcome the charging energy E_C to add one more electron to the QD, it produces a photocurrent in the blue colored regions of the Coulomb diamond shown in Figure 3(c). Therefore, as V_G is swept at V_{DS} = 0, the photocurrent mechanism changes from the N↔N-1 excitation to the N↔N+1 excitation, as shown in Figure 3(d). The total photocurrent, I_p, is expressed as;

$$I_p = f_{N-1} I_{N-1} + f_{N+1} I_{N+1} \quad (1)$$

where I_{N-1} (red curve in Figure 3(d)) and I_{N+1} (blue curve in Figure 3(d)) correspond to the photocurrent generated by the N↔N-1 and N↔N+1 excitation processes, respectively, and f_{N-1} and f_{N+1} correspond to the probabilities for the SET to return to the initial state through the N↔N-1 and N↔N+1 excitation processes, respectively. When V_G is swept, the total photocurrent I_p varies, as shown by the black dashed line in Figure 3(d).

As we can see in Figures 1(c), 1(e) and 1(g), the photocurrent changes with V_G even within a Coulomb diamond. When the photocurrent mechanism changes, the photocurrent may become smaller (as shown by P_A in Figure 1(c)) or larger (as shown by P_B in Figure 1(e)), or may even change its polarity (as shown by P_C in Figure 1(g)). The difference originates from the fact that, for the N↔N-1 excitation, the photoexcited electron tunnels out when N electrons reside in the dot, whereas, for the N↔N+1 excitation, the photoexcited electron tunnels out when N+1 electrons reside in the dot. Even when the intersublevel transition in the QD is the same, the manybody wavefunctions of the excited state are different when the tunneling takes place in the two excitation processes. This results in different tunneling asymmetry ratios and, hence, different photocurrents.

Let us now look more closely at the photocurrent when a finite source-drain voltage, V_{DS} is applied. As shown in Figures 1(h) and 1(i), the photocurrent displays a staircase-like increase with

increasing V_{DS}. Figure 4(a) shows the photocurrent spectra measured on sample C for various V_{DS} at V_G = 510 mV, corresponding to the photocurrent shown in Figure 1(i). As indicated by red arrows, the photocurrent peak at 15 meV changes its polarity from negative to positive and becomes larger with increasing V_{DS}, while other structures are not much affected. This confirms that the photocurrent increase with V_{DS} does not result from the excitation of other transition lines, but mainly arises from the enhancement of one of the transition peaks.

The stepwise increase in the photocurrent is due to the tunnel blocking by the electrodes. The tunnel escape or filling of an electron in the direction opposite to the net electron flow reduces the photocurrent. Such an opposite tunneling flow can be blocked by applying an appropriate V_{DS}, resulting in a photocurrent enhancement. For example, in the case of the $N \leftrightarrow N$-1 excitation, we can block the tunnel escape of the photoexcited electron to the source by applying a positive V_{DS}, as shown in Figure 4(b) (the Fermi level blocking). In the case of the $N \leftrightarrow N$+1 excitation, when V_{DS} = 0, the empty lower energy state can be filled either from the source or drain electrodes, as shown in Figure 4(c). However, by applying a positive V_{DS}, we can block the filling of electrons from the drain, because the Fermi level of drain electrode is not high enough to provide the required charging energy, E_C, for the filling process, as shown in Figure 4(d) (the charging energy blocking). Therefore, the step-like increase in photocurrent appears when the *empty* upper energy state in the $N \leftrightarrow N$-1 excitation or the *filled* lower energy state in the $N \leftrightarrow N$+1 excitation enters the source-drain Fermi level window.

Finally, we would like to make a comment on a potential application of the THz photovoltaic effect to nanoscale energy harvesting. Recently, it has been demonstrated that QDs can generate electricity from waste heat and electrical noise.[20, 21] The present THz photovoltaic effect has a similar function of converting blackbody radiation into electrical power. The internal quantum efficiency for resonant photoexcitation estimated from the measured tunneling asymmetry is in the order of 10%-50% for samples A- C. The gate-controllability may add further functionality to the device.

In summary, we have observed a THz induced single electron photovoltaic effect in self-assembled InAs QDs. We used a SET geometry that consists of a single InAs QD and nanogap electrodes coupled to a bowtie antenna. Under a weak, broadband THz radiation, a photocurrent induced by THz intersublevel transitions in the QD is generated even when no bias voltage is applied to the SET. The observed single electron photovoltaic effect originates from an energy-dependent tunneling asymmetry in the QD-SET. Moreover, the tunneling asymmetry changes not only with the shell, but also with the electron number in the QD, suggesting the manybody nature of the electron wavefunctions. When a finite source-drain voltage is applied to the SET, the photocurrent is found to increase stepwise, which we attribute to the blocking of the electron tunneling by the electrodes. The THz photovoltaic effect observed in the present QD-SET system has an internal quantum efficiency of the order of 10%-50% for resonant photoexcitation and is gate-controllable, suggesting potential applications to nanoscale energy harvesting.

We thank Y. Arakawa for his fruitful discussions and continuous encouragement. This work was partly supported by CREST-JST, Grants-in-Aid from JSPS (No. 25246004, No. 25600013, and No. 26706002), Project for Developing Innovation Systems of MEXT, and research grants from the Canon Foundation and the Casio Science Foundation. G.B. gratefully acknowledges IIS, University of Tokyo, for support. C.N.-B. thanks JSPS/CNRS for support. Y.Z. gratefully acknowledges the support from the Yoshida Scholarship Foundation.

Reference

[1] M. A. Kastner, Phys. Today **46**, 24 (1993).

[2] R.C. Ashoori, Nature **379**, 413 (1996).

[3] P. M. Petroff, A. Lorke, and A. Imamoglu, Phys. Today **54**, 46 (2001).

[4] M. A. Kastner, Rev. of Mod. Phys. **64**, 849 (1992).

[5] S. Tarucha, D. G. Austing, T. Honda, R. J. Van der Hage, and L. P. Kouwenhoven, Phys. Rev. Lett. **77**, 3613 (1996).

[6] M. Jung, K. Hirakawa, Y. Kawaguchi, S. Komiyama, S. Ishida, and Y. Arakawa, Appl. Phys. Lett. **86**, 033106 (2005).

[7] C. Buizert, A. Oiwa, K. Shibata, K. Hirakawa, and S. Tarucha, Phys. Rev. Lett. **99**, 136806.

[8] R. S. Deacon, Y. Tanaka, A. Oiwa, R. Sakano, K. Yoshida, K. Shibata, K. Hirakawa, and S. Tarucha, Phys. Rev. Lett. **104**, 076805 (2010).

[9] Y. Kanai, R. S. Deacon, S. Takahashi, A. Oiwa, K. Yoshida, K. Shibata, K. Hirakawa, Y. Tokura, and S. Tarucha, Nat. nanotech. **6**, 511 (2011).

[10] K. Shibata, H. Yuan, Y. Iwasa, and K. Hirakawa, Nat. commun. **4**, 2664(2013).

[11] M. Jung, T. Machida, K. Hirakawa, S. Komiyama, T. Nakaoka, S. Ishida, and Y. Arakawa, Appl. Phys. Lett. **87**, 203109 (2005).

[12] Y. Zhang, K. Shibata, N. Nagai, C. Ndebeka-Bandou, G. Bastard, and K. Hirakawa, Nano Lett. **15(2)**, 1166 (2015).

[13] Y. Zhang, K. Shibata, N. Nagai, C. Ndebeka-Bandou, G. Bastard, and K. Hirakawa, Phy. Rev. B **91**, 241301(R) (2015).

[14] W. Ma, R. Nötzel, H.-P. Schönherr, and K. H. Ploog, Appl. Phys. Lett. **79**, 4219 (2001).

[15] K. Shibata, K. Seki, P. J. J. Luukko, E. Räsänen, K. M. Cha, I. Horiuchi, and K. Hirakawa, Appl. Phys. Lett. **99**, 182104 (2011).

[16] K. Shibata, K. Seki, P. J. J. Luukko, E. Räsänen, S. Schnez, T. Ihn, K. Ensslin, and K.Hirakawa, Appl. Phys. Exp. **7**, 045001 (2014).

[17] K. Shibata, A. Umeno, K. M. Cha, and K. Hirakawa, Phys. Rev. Lett. **109**, 077401 (2012).

[18] E. A. Zibik, T. Grange, B. A. Carpenter, N. E. Porter, R. Ferreira, G. Bastard, D. Stehr, S. Winnerl,

M. Helm, H. Y. Liu, M. S. Skolnick, and L. R. Wilson, Nat. Mater., **8**, 803 (2009).

[19] See http://www.nextnano.com/ for more information about *Nextnano*; accessed: 19 August, 2015.

[20] R. Sánchez, and M. Büttiker, Phys. Rev. B **83**, 085428 (2011).

[21] F. Hartmann, P. Pfeffer, S. Höfling, M. Kamp, and L. Worschech, Phys. Rev. Lett. **114**, 146805(2015).

Figure Captions

FIG. 1. (a) Schematic cross section of the QD-SET sample mounted on a Si solid immersion lens. (b) Coulomb stability diagram of sample A. White solid lines are eyeguides for the boundaries of the Coulomb diamonds. White dashed lines denote the excited states. The number in the Coulomb diamonds denotes the number of electrons in the dot. (c) THz-induced photocurrent as a function of V_G measured on sample A by applying a small source-drain voltage (V_{DS} = 0.25 mV). P_A indicates the gate voltage where the $N \leftrightarrow N+1$ excitation process starts contributing to the photocurrent. Points P_B and P_C in (e) and (g), respectively, have the same meaning. (d) Coulomb stability diagram of sample B. (e) THz-induced photocurrent as a function of V_G measured at V_{DS} = 0.25 mV on sample B. (f) Coulomb stability diagram of sample C. (g) THz-induced photocurrent as a function of V_G measured at V_{DS} = 0.25 mV on sample C. (h) Photocurrent as a function of V_{DS} measured on sample B at V_G = 1450 mV and 1550 mV. (i) Photocurrent as a function of V_{DS} measured on sample C at V_G = 510 mV.

FIG. 2. (a) Energy band diagram of a QD-SET. Γ_P is the THz photoexcitation rate in the QD. Γ_{ES} (Γ_{FS}) and Γ_{ED} (Γ_{FD}) are the tunnel escape (filling) rates of an electron to (from) the source and drain electrodes, respectively. The red arrow indicates the net electron flow through the SET. The size of the arrows schematically denotes the magnitude of the tunnel couplings. (b) and (c) Schematic cross sections of a QD-SET sample and the wavefunction patterns calculated for the p- and d-shells, respectively, assuming that the dot has a cone shape that is slightly elongated in the direction of the source-drain electrodes (84L×80W×16H nm^3). $\Gamma_{S(p)}$ and $\Gamma_{D(p)}$ express the tunneling rate of the p-states to the source and drain electrodes, respectively. Similarly, $\Gamma_{S(d)}$ and $\Gamma_{D(d)}$ have the same meanings for the d-states.

FIG. 3. (a) The energy band diagrams for the three-step $N \leftrightarrow N-1$ photoexcitation process. ΔE and E_C denote the energy level separation and the charging energy, respectively. Γ_E and Γ_R denote the tunnel escape rate and the relaxation rate, respectively. GS and ES stand for the ground and excited states, respectively. (b) The energy band diagrams for the three-step $N \leftrightarrow N+1$

photoexcitation process. (c) The allowed regions for the $N \leftrightarrow N$-1 and $N \leftrightarrow N$+1 photoexcitation processes are indicated in pink and blue, respectively. (d) Schematic illustration of the expected V_G-dependence of the photocurrent at V_{DS} = 0. The blue, red, and dashed lines express the photocurrent generated by the $N \leftrightarrow N$-1 excitation, $N \leftrightarrow N$+1 excitation, and the total processes, respectively.

FIG. 4. Photocurrent spectra measured at V_G = 510 mV on sample C, which corresponds to the photocurrent data shown in Figure 1(i). (b) Mechanism for the photocurrent change induced by the Fermi level blocking in the $N \leftrightarrow N$-1 excitation process. The red bold arrows indicate the net electron flows through the SET. The size of the arrows schematically indicates the magnitude of the electron flow. (c) Schematic illustration of the photocurrent generated by the $N \leftrightarrow N$+1 excitation when V_{DS} = 0. E_C expresses the charging energy required for filling the empty lower energy state in the QD. (d) Mechanism for the photocurrent change induced by the charging energy blocking in the $N \leftrightarrow N$+1 excitation process.

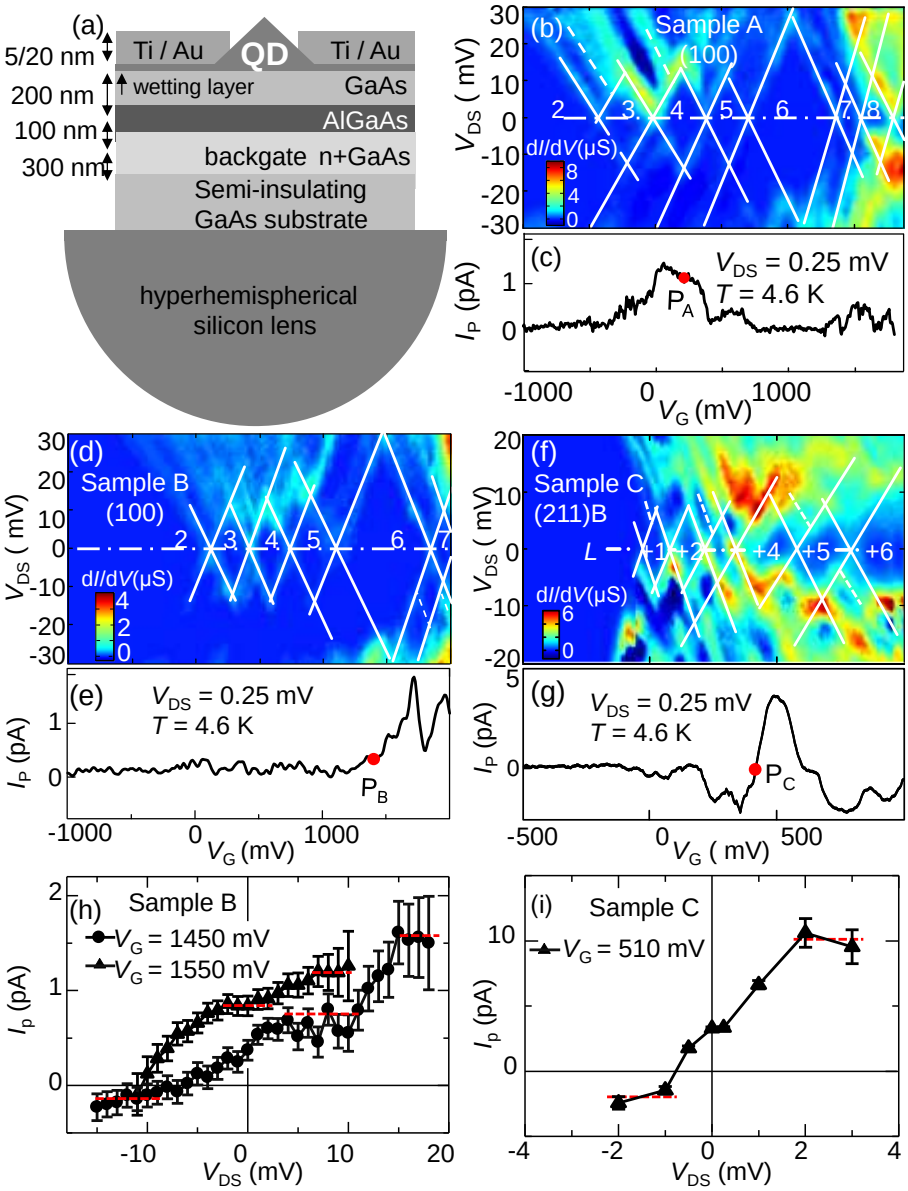

Fig. 1 Y. Zhang, et al.

APL

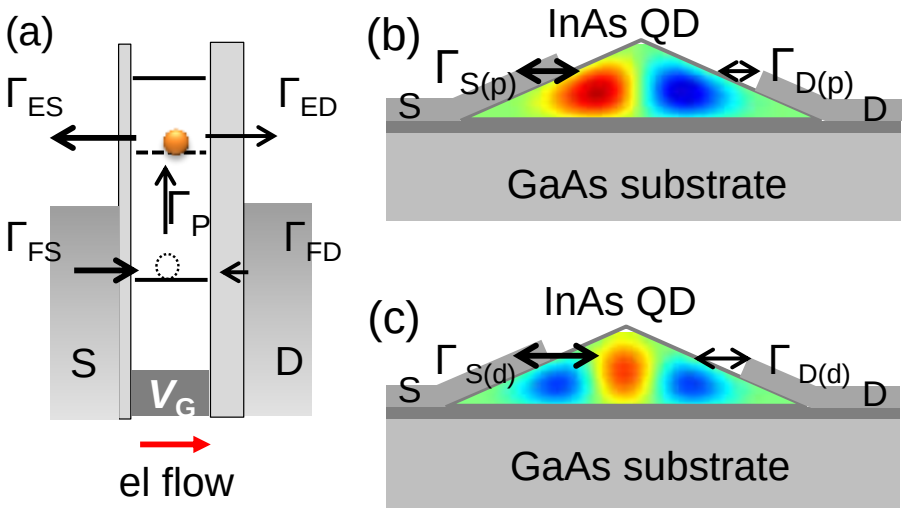

Fig. 2 Y. Zhang, et al.

APL

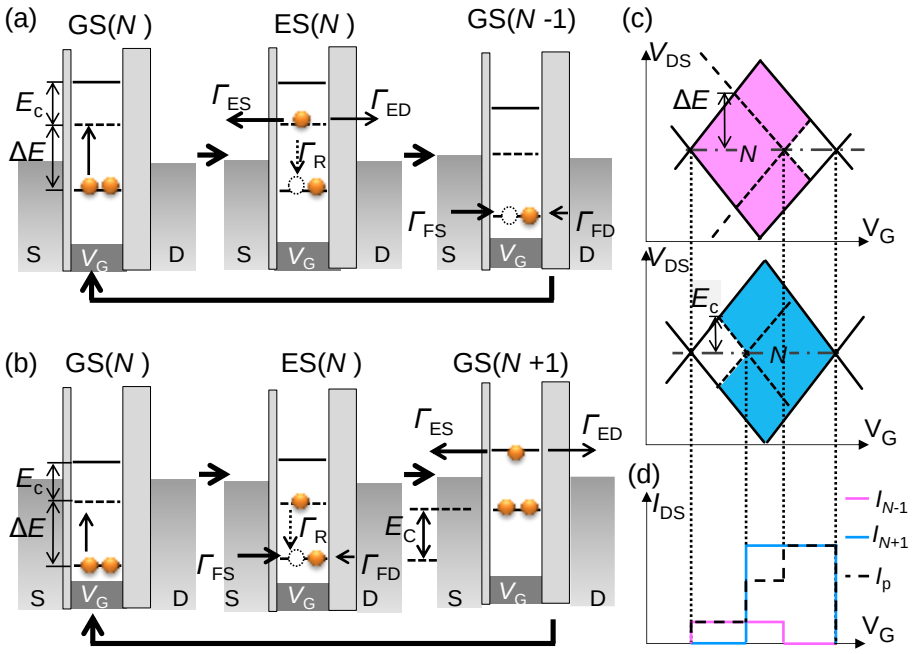

Fig. 3 Y. Zhang, et al.

APL

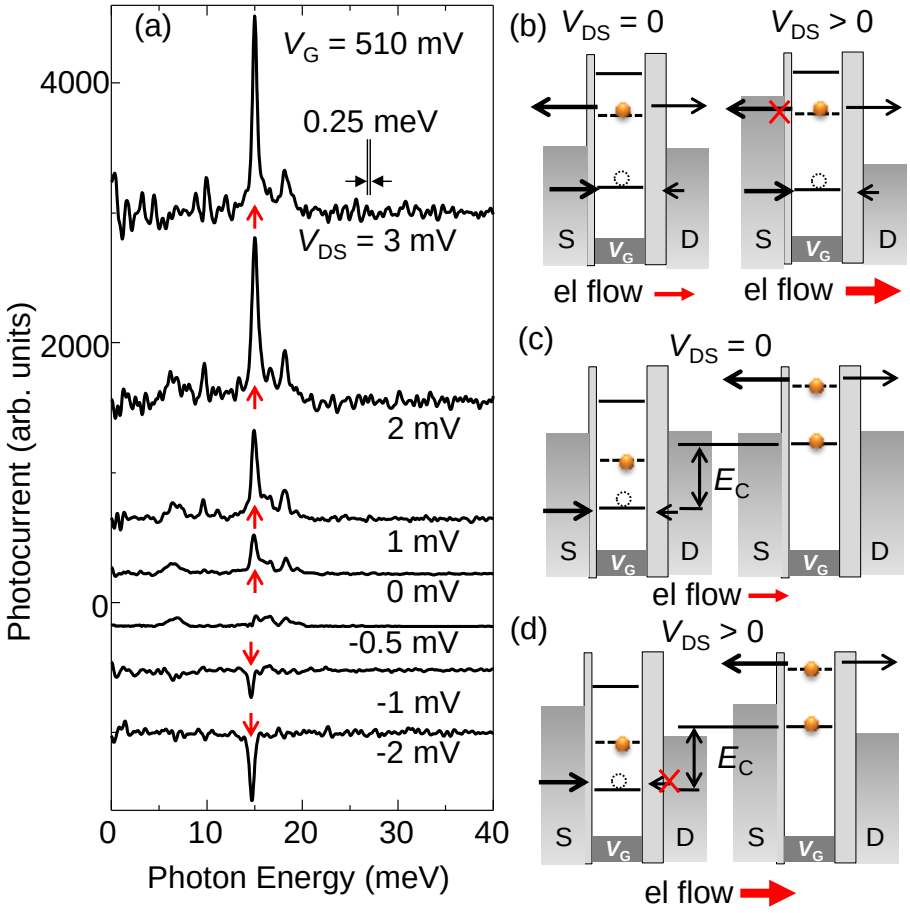

Fig. 4 Y. Zhang, et al.

APL